Physica B 588 (2020) 412178

Contents lists available at ScienceDirect

Physica B: Physics of Condensed Matter

journal homepage: http://www.elsevier.com/locate/physb

Transport and thermoelectric performance of *n*-type PbTe films

B. Dzundza [a], L. Nykyruy [a], T. Parashchuk [b,*], E. Ivakin [c], Y. Yavorsky [a], L. Chernyak [d], Z. Dashevsky [e]

[a] Vasyl Stefanyk Precarpathian National University, Ivano-Frankivsk, Ukraine
[b] The Lukasiewicz Research Network – the Institute of Advanced Manufacturing Technology, Krakow, Poland
[c] Belarusian State University, Minsk, Belarus
[d] Department of Physics, University of Central Florida, USA
[e] Department of Materials Engineering, Ben-Gurion University of the Negev, Beer-Sheva, Israel

ARTICLE INFO

Keywords:
Thin films
Lead telluride
Thermoelectrical properties

ABSTRACT

In the present work, a systematic study of structural, transport, and thermoelectric properties of *n*-PbTe films on a mica substrate has been carried out. A wide range of film samples with hole concentration from $n = 8 \times 10^{16}$ cm^{-3} to $n = 3 \times 10^{18}$ cm^{-3} were obtained by variation of composition of the stoichiometric PbTe and by additional doping with donor iodine impurity. Based on measurements obtained by the four coefficients method, the direct estimation of the density of states effective mass and the scattering mechanism of the investigated *n*-PbTe films has been carried out. The high thermoelectric figure of merit $Z \approx 1.3 \times 10^{-3}$ K^{-1} at $T = 300$ K has been obtained. Such a high thermoelectric figure of merit Z for *n*-PbTe films opens a possibility for the fabrication of the Film Thermoelectric Modules (FTEM), which could be a candidate for application at micro-scale thermoelectric converters.

1. Introduction

IV-VI compounds are extremely interesting semiconductors with unusual and unique properties in comparison with other semiconductors. For more than thirty years, these materials have been the subject of considerable research effort due to both interest in the fundamental physics of these semiconductors and their technological importance [1–10]. The technological interest in IV-VI semiconductors, especially in the lead salts, originates from their current and potential use for thermoelectricity.

The efficiency of heat conversion to electricity is determined by the thermoelectric figure of merit Z:

$$Z = \frac{S^2\sigma}{\kappa}, \quad (1)$$

where S is the Seebeck coefficient, σ and κ are the electrical and thermal conductivities, respectively.

Therefore, an effective thermoelectric material should correspond with the following criteria [11]:

1. Semiconductor material (elemental, compound, alloy, composite, multilayer, superlattice, low-dimensional structure) should preferably consist of heavy atoms. It will cause a low frequency of thermal vibrations of a lattice and a significant decrease in the lattice thermal conductivity κ_L.
2. Semiconductor material should have high dielectric constant $\varepsilon > 100$, which reduces the scattering of charge carriers by impurity ions and small effective mass of major charge carriers (electrons for *n*-type and heavy holes for *p*-type). These two criteria provide high mobility of charge carriers μ.

It should be noted that high dielectric constant ε leads to a decrease in the ionization energy of the impurity atoms (which is practically approaching zero). As a result, energy level of impurity merges with the conduction or valence band, and concentration of electrons in the conduction band of *n*-type material or concentration of heavy holes in the valence band of *p*-type material becomes constant (similar to metallic conductivity) and equals the dopant concentration in the temperature range from 0 K to the onset of intrinsic conductivity.

* Corresponding author. Center of Thermoelectric Materials Analyzes, The Lukasiewicz Research Network – The Institute of Advanced Manufacturing Technology, Wrocławska 37A, 30-011, Krakow, Poland.
E-mail addresses: taras.parashchuk@kit.lukasievich.krakow.pl, taras.parashchuk@kit.lukasiewicz.gov.pl (T. Parashchuk).

https://doi.org/10.1016/j.physb.2020.412178
Received 29 January 2020; Received in revised form 13 February 2020; Accepted 29 March 2020
Available online 8 April 2020

3. Semiconductor materials should have a high degeneracy of the conduction band for *n*-type and the same valence band degeneracy for *p*-type. In this case, the concentration of charge carriers increases significantly without changing the Fermi level E_F position because it is directly proportional to the number of ellipsoids and, therefore, the electrical conductivity shows a significant growth up as well.
4. The solubility limit for doping elements in semiconductor must be high, ensuring the achievement of large concentrations of charge carriers $n(p) > 10^{19}$ cm^{-3}. Consequently, the optimal Fermi level energy E_F ($E_F - E_C$) ~ 0 eV for *n*-type and ($E_V - E_F$) ~ 0 eV for *p*-type, and maximum value of power factor $P = S^2\sigma$ could be obtained.
5. Band gap E_g of the semiconductor in the operating temperature range of thermoelectric material should be $E_g > 8k_0T$ to minimize the contribution of thermally generated minority charge carriers to total electrical conductivity, leading to a decrease in thermoelectric efficiency.

Recently, there has been a strong need for the microelectronic applications with few microwatts power at relatively high voltage for the operation of small electric. For this purpose, a film thermoelectric module (generator) (FTEC), which consists of *n*- and *p*-type film legs, connected at the series circle and fabricated on a thin isolate substrate, could be used [12,13]. The output power of such FTECs is in the range from 100 nW to 10 mW [14–17].

The high sensitivity of FTECs allows them to operate efficiently at small temperature differences. In this case, a human body whose temperature differs from the ambient temperature can be used as a source of heat [18,19]. As noted above, PbTe is one of the useful thermoelectric materials, and therefore, the goal of this research is the fabrication of PbTe films with optimal thermoelectric parameters similar to the bulk crystals.

2. Experimental

For film fabrication, stoichiometric PbTe material has been used. The deviations from stoichiometry have been performed, aiming to modify the concentration of PbTe-based composition. Compound semiconductors usually exist in a solidus field around perfect stoichiometry. When metal-rich, PbTe is *n*-type due to either Te vacancies or Pb interstitials, which act as donors [20–22]. In this case, the $Pb_{1.001}Te_{0.999}$ composition has been used. For the preparation of PbTe films with higher electron concentration, PbTe doped with iodine donor impurity ($PbTe_{0.999}I_{0.001}$) composition was prepared [6]. Therefore, a set of samples with the concentration at T = 300 K $n = 8 \times 10^{16}$ cm^{-3}, 3×10^{17} cm^{-3}, 5×10^{17} cm^{-3}, 2×10^{18} cm^{-3}, 3×10^{18} cm^{-3} has been prepared.

Synthesis of PbTe-based materials was carried out by direct melting of components for 10 h at 1073 K in sealed quartz ampoules evacuated to a residual pressure of 10^{-5} mbar. Then each ampoule was taken from the furnace and quenched into cold water. The synthesis was carried out using high-purity initial components — Pb (99.999), Te (99.9999), and PbI_2 (99.999. The resultant ingots were crushed into fine powders by ball milling in an argon atmosphere.

The *n*-type PbTe thin films were deposited using open vacuum evaporation technology. The temperature of the substrate for film preparation was $T_s = 523$ K; evaporation velocity was $v_e = 0.1$ μm/min. After the evaporation process, all films were annealed at the same evaporation chamber and at $T_t = 623$ K for 0.5 h in the atmosphere of pure argon under the pressure of $p = 0.9$ atm. All films were prepared on a thin mica substrate with a thickness of ~10 μm.

The X-ray diffraction characterization was performed with a high-resolution Bede D3 diffractometer coupled to a Rigaku rotating anode generator (18 kW) providing CuKα radiation. The scans in double-axis mode were measured with a Bartels two-channel cut Si (220) monochromator in the primary beam and the reciprocal space mapping in triple-axis mode the one channel-cut analyzer crystal in (220) asymmetrical stetting was introduced in the diffracted beam path. The analysis of the chemical composition of the PbTe films was made on the Auger-microanalyser "JAMP-10". Measurement of the Seebeck coefficient *S* on a bulk material is based on the formation of the temperature gradient across the whole bulk material and simple probing of each side of the sample. However, due to radiation, convection, uncontrolled heating by electrodes and the substrate effect on the distribution of the heat, there is no suitable and convenient methodology for measuring the Seebeck coefficient for thin films. Therefore, the measurement of the Seebeck coefficient on the thin film requires some alternative approach [23]. For the investigation of the Seebeck coefficient *S* on thin films at close to room temperature (T ~ 300 K), the original measurement setup has been developed. The schematic view of the device with the description of the measurement approach is shown in Appendix A, Fig. 7. The accuracy of measuring the Seebeck coefficient using the developed setup did not exceed ~1%.

For the investigation of the transport properties on thin films (Seebeck coefficient *S*, electrical conductivity σ, Hall coefficient R_H, and transverse Nernst coefficient *Q*) over a broad temperature range (80–400 K), a measurement setup has been developed. The scheme of the device with the description of the measurement approach is shown in Appendix B, Fig. 8(a and b). The measurement of Hall and transverse Nernst effects was carried out in permanent magnetic fields up to 2 T. The results are averaged measurements in two directions of the electrical and magnetic fields. The accuracy of the temperature measurement was 0.1–0.2 K, and of the magnetic field ±3%. The uncertainty of the Seebeck coefficient and electrical conductivity measurements was 6%. The Hall effect was measured with an accuracy of 8% and the transverse Nernst effect – with an accuracy of 10%.

The investigation of heat transfer in *n*-PbTe films on flexible substrate is performed by the method of dynamic lattices [23]. It is based on the effect that the sample is excited by two mutually interfering laser beams. As a result, the samples are characterized by dynamic diffraction lattice, and the kinetics of the diffraction signal could be analyzed. Finally, using such a method, the value of thermal diffusivity α was measured. The uncertainty of the thermal diffusivity measurement was not more than 10%. The schematic view of the device with the description of the measurement approach is shown in Appendix C, Fig. 9. The total thermal conductivity was calculated according to the following formula:

$$\kappa = \alpha \rho c_p, \tag{2}$$

where ρ is the single crystal density and c_p is the specific heat capacity calculated within the Dulong-Petit limit.

3. Results and discussion

3.1. Structural properties

The measured rocking curves for various PbTe reflections are shown in Fig. 1 and their Full Width at Half Maximum (FWHM) varied in the range 120–160 arcsec. This XRD method is an important tool for epitaxial growth determination of PbTe films on monocrystalline (single

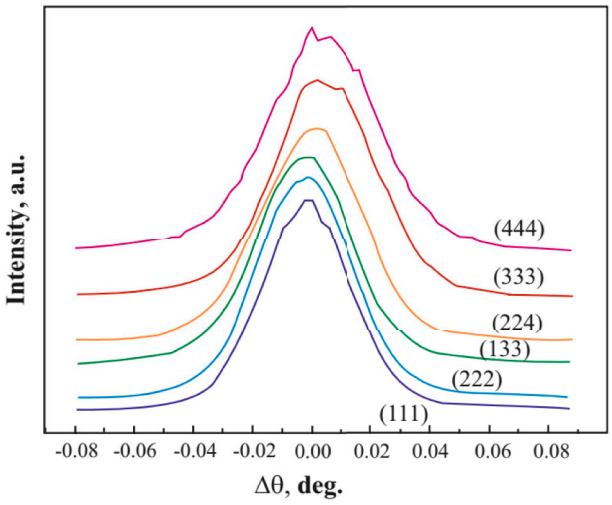

Fig. 1. The normalized rocking curves measured for various peaks of a 5 μm thick (111) oriented PbTe layer on (0001) mica substrate. The profiles are displaced for clarity of the picture.

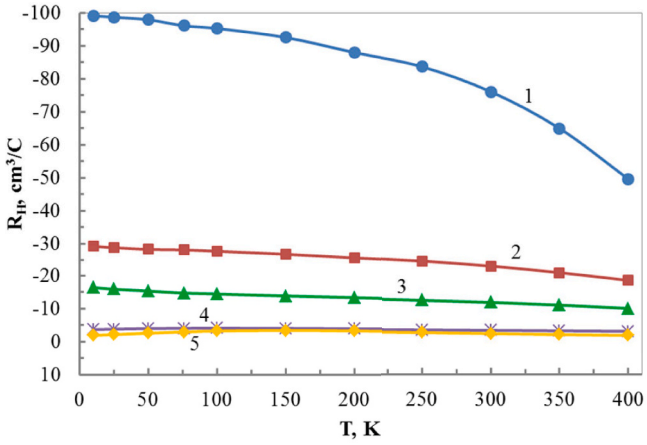

Fig. 2. Hall coefficient as a function of temperature for *n*-PbTe films. 1–8 × 10^{16} cm^{-3}, 2–3 × 10^{17} cm^{-3}, 3–5 × 10^{17} cm^{-3}, 4–2 × 10^{18} cm^{-3}, 5–3 × 10^{18} cm^{-3}.

crystal) mica substrate [24]. As was determined from the standard θ:2θ scan the epitaxial orientation of the PbTe layer grown on the mica substrate corresponds to (111) PbTe plane parallel to (0001) mica substrate.

3.2. Transport properties

Fig. 2 demonstrates the temperature dependence of the Hall coefficient R_H from 10 K to 400 K for *n*-PbTe films. All films have the negative values of the Hall coefficient over the entire temperature range, which is related to electronic conductivity (*n*-type) in PbTe films. The carrier concentration for prepared PbTe films has been determined using the following expression:

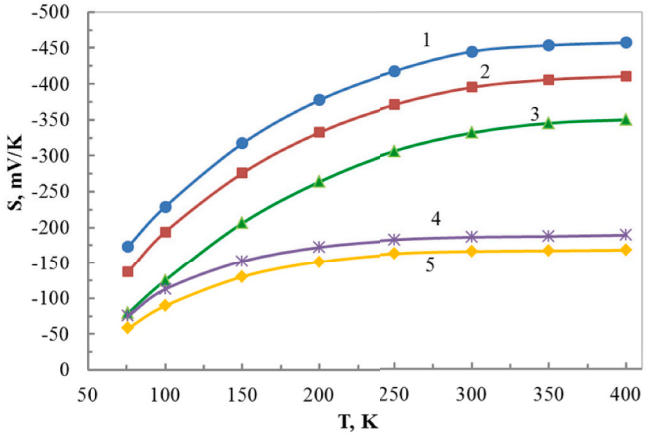

Fig. 3. Seebeck coefficient as a function of temperature for *n*-PbTe films. 1–8 × 10^{16} cm^{-3}, 2–3 × 10^{17} cm^{-3}, 3–5 × 10^{17} cm^{-3}, 4–2 × 10^{18} cm^{-3}, 5–3 × 10^{18} cm^{-3}.

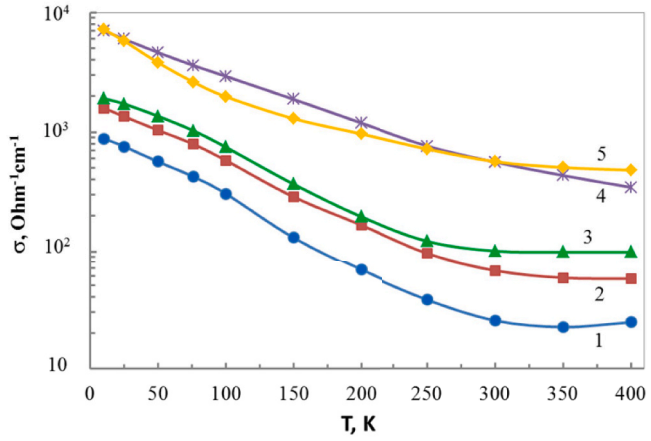

Fig. 4. Electrical conductivity as a function of temperature for *n*-PbTe films. 1–8 × 10^{16} cm^{-3}, 2–3 × 10^{17} cm^{-3}, 3–5 × 10^{17} cm^{-3}, 4–2 × 10^{18} cm^{-3}, 5–3 × 10^{18} cm^{-3}.

$$n = \frac{1}{eR_H}, \tag{3}$$

where *e* is the charge of an electron.

The Seebeck coefficient for all films also has negative values over the investigated temperature range, which is typical for semiconductors with an electron type of conductivity (Fig. 3).

Fig. 4 demonstrates the temperature dependence of electrical conductivity σ over the entire temperature range for *n*-type PbTe films. The value of σ is increasing with the growth of the carrier concentration *n* from 80 to 400 K. The temperature dependence of σ for *n*-PbTe films shows decreases indicating metal-like conductivity.

Hall mobility has been calculated within the following expression and represented in Fig. 5:

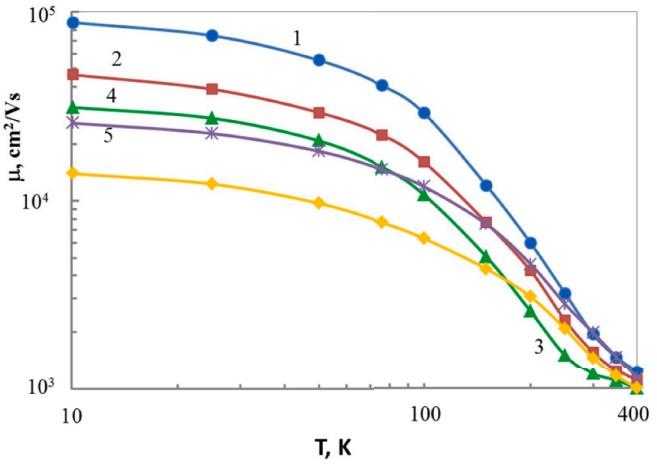

Fig. 5. Hall mobility as a function of temperature for *n*-PbTe films. 1–8 × 10^{16} cm^{-3}, 2–3 × 10^{17} cm^{-3}, 3–5 × 10^{17} cm^{-3}, 4–2 × 10^{18} cm^{-3}, 5–3 × 10^{18} cm^{-3}.

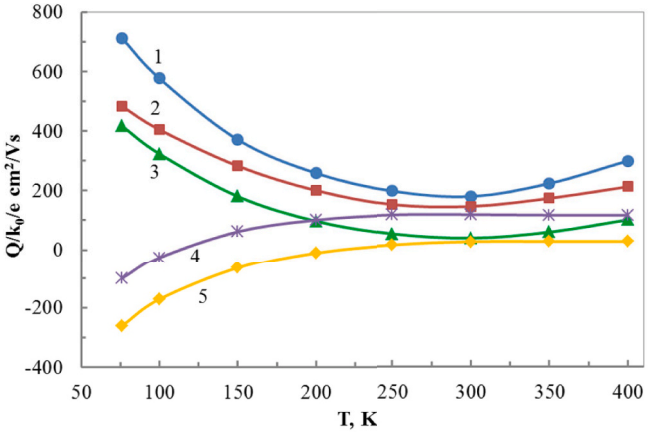

Fig. 6. Transverse Nernst coefficient as a function of temperature for *n*-PbTe films. 1–8 × 10^{16} cm^{-3}, 2–3 × 10^{17} cm^{-3}, 3–5 × 10^{17} cm^{-3}, 4–2 × 10^{18} cm^{-3}, 5–3 × 10^{18} cm^{-3}.

$$\mu_H = R_H\sigma. \tag{4}$$

At low temperature, Hall mobility for *n*-PbTe films with Hall concentration $n \sim 8 \times 10^{16}$ cm^{-3} (sample 1) achieves the value of 7.4×10^4 cm^2/V, which is comparable with available data for the best epitaxial *n*-PbTe films, prepared by Molecular Beam Epitaxy (MBE) on BaF_2 substrate [25]. With increasing temperature μ_H decreases for about the order of magnitude for all investigated samples, while the scaling of mobility with temperature $\mu_H \sim T^{-\beta}$ shows a value of $\beta = 1.2$–1.4 at high temperatures. Such values correspond to the scattering of electrons on the acoustic phonons. Generally, the dependence σ(T) and μ_H(T) for *n*-PbTe films are similar to bulk *n*-PbTe single crystals.

Fig. 6 shows the temperature dependence of the transverse Nernst coefficient *Q* from 80 to 400 K for *n*-PbTe films. The sign of the transverse Nernst coefficient *Q* at low temperature reveals an inverse energy dependence on the relaxation time, indicating a phonon scattering in the parabolic band and degenerate semiconductors [26]. For some samples with low carrier concentration, a positive value of *Q* has been observed due to the influence of minority carriers (holes). It is common since the transverse Nernst coefficient is the most sensitive from three other parameters (the Hall coefficient, the Seebeck coefficient, and electrical conductivity) for the indication of the beginning of the intrinsic state [5].

3.3. Scattering parameter and density of states effective mass

Mean free path in the case of the parabolic zone and for charge carriers is $l = l_0E^r$, where l_0 is constant, *E* is charge carrier energy, *r* is scattering parameter. The Seebeck coefficient *S* is defined as [3,6]:

$$S = \frac{k_0}{e}\left[\frac{(r+2)F_{r+1}(\mu^*)}{(r+1)F_r(\mu^*)} - \mu^*\right], \tag{5}$$

where k_0 is the Boltzmann constant, $F_r(\mu^*)$, and $F_{r+1}(\mu^*)$ are Fermi-Dirac integrals, parameter $\mu^* = (E_F - E_V)/k_0T$ is the reduced Fermi energy. Here E_V is the valence band maximum, E_F is the Fermi level, and *T* is the absolute temperature.

In a strong magnetic field, the Seebeck coefficient *S* is isotropic, which means it does not depend on the scattering mechanism, and it is a function of the reduced chemical potential only:

Table 1
Carrier concentration *n*, carrier mobility μ, effective mass m^*/m_0 and scattering parameter *r* for *n*-PbTe films at 100 K.

Sample	Composition	*n*, cm^{-3}	μ_H, $cm^2V^{-1}s^{-1}$	m^*/m_0	*r*
1	PbTe	8×10^{16}	29,000	0.24	0
2	PbTe	2×10^{17}	16,000	0.24	0
3	$Pb_{1.001}Te_{0.999}$	6×10^{17}	11,000	0.245	0
4	$PbTe_{0.999}I_{0.001}$	2×10^{18}	10,000	0.25	0
5	$PbTe_{0.999}I_{0.001}$	3×10^{18}	6000	0.26	0.1

$$S = \frac{k_0}{e}\left[\frac{5F_{5/2}(\mu^*)}{3F_{1/2}(\mu^*)} - \mu^*\right]. \tag{6}$$

The density of states effective mass m^* and the scattering parameter *r* can be directly determined from a set of four kinetic coefficients *S*, σ, R_H, and *Q* [26]:

$$m^* = \left(\frac{3n}{\pi}\right)^{2/3}\frac{e\hbar^2}{k_0^2T}\left(S - \frac{Q}{|R|\sigma}\right), \tag{7}$$

$$r = \frac{Q/|R|\sigma}{S - Q/|R|\sigma}. \tag{8}$$

Using Eqs. (5)–(8) effective mass m_* and scattering parameter *r* have been determined for *n*-PbTe films at 100 K. For all films, at a given temperature, the scattering parameter *r* is close to ≈0. This value is characterized by a mechanism of carrier scattering on acoustic phonons [3,4], which is typical for high-performance bulk *n*-PbTe bulk samples. The m^*/m_0 (m_0 is the mass of a free electron) values calculated using data of *S*, *Q*, *R*, and σ for *n*-PbTe films at 100 K increase slightly from 0.24 to 0.26 with the increasing of the concentration *p* (Table 1). This effect can be connected with the non-parabolic shape of the conduction band at PbTe [4].

3.4. Thermoelectric properties

Table 2 demonstrates thermoelectric properties (Seebeck coefficient *S*, electrical conductivity σ and thermal conductivity κ) at $T = 300$ K for five *n*-PbTe films on a mica substrate with a thickness of 5 ± 0.5 μm and

Table 2
Thermoelectric properties of *n*-PbTe films and bulk crystals at $T = 300$ K.

Hall concentration *n*, cm-3	Type of material	Seebeck coefficient *S*, μV/K	Electrical conductivity σ, Ω-1cm-1	Thermal conductivity κ, W/cm K	Lattice thermal conductivity κl, W/cm K	Figure of merit *Z* x 103, K-1	Ref.
8×10^{16}	film	−450	25	19×10^{-3}	19×10^{-3}	0.3	
3×10^{17}	film	−400	70	18×10^{-3}	18×10^{-3}	0.6	
5×10^{17}	film	−330	100	18.5×10^{-3}	18×10^{-3}	0.6	
2×10^{18}	film	−185	700	21×10^{-3}	18×10^{-3}	1.1	
3×10^{18}	film	−165	1100	23×10^{-3}	18×10^{-3}	1.3	
	bulk	−200	600	23×10^{-3}	20×10^{-3}	1.2	[3]
	bulk	−200	1000	25×10^{-3}	20×10^{-3}	1.5	[6]

different compositions. The thermoelectric parameters of the bulk *n*-type PbTe crystals taken from Refs. [3,6] also are shown in Table 2. The calculated thermoelectric figure of merit *Z* for the *n*-PbTe film with the concentration $n = 3 \times 10^{18}$ cm^{-3} achieves the value $Z \approx 1.3 \times 10^{-3}$ K^{-1} at 300 K, which is close to *Z* value for *n*-PbTe bulk crystals.

Heat transport is determined by total thermal conductivity κ_{tot} of semiconductor, which consists of three components: the lattice thermal conductivity of phonons κ_l, the electronic thermal conductivity of free electrons κ_e and the ambipolar thermal conductivity of electron-hole pairs κ_a in the intrinsic conduction region [4,6]:

$$\kappa_{tot} = \kappa_l + \kappa_e + \kappa_a. \quad (9)$$

For one type of carriers (holes) at the majority area, only two first coefficients of thermal conductivity influence the value of κ. The total thermal conductivity κ at $T = 300$ K was measured and shown in Table 2. The values of κe have been obtained using Wiedemann-Franz law:

$$\kappa_e = L_0 \sigma T, \quad (10)$$

where *L* is the Lorentz number, which can be calculated using the following equation [6]:

$$L = \left(\frac{k_0}{e}\right)^2 \left[3\frac{F_2(\mu^*)}{F_0(\mu^*)} - \left(2\frac{F_2(\mu^*)}{F_0(\mu^*)}\right)^2\right], \quad (11)$$

At the acoustic phonon scattering of charge carriers, the reduced Fermi energy μ* can be obtained from fitting the Seebeck coefficient using equation (5).

The lattice thermal conductivity κl was calculated according to eq. (9) and also represented in Table 2. Obviously, that the values of lattice thermal conductivity are very similar for all films. This can be explanined by the fact, that an increase in the carrier concentration due to doping of a semiconductor does not affect on the lattice term of the thermal conductivity, but changes the electronic part of the thermal conductivity due to an increase in electrical conductivity (Wiedemann-Franz law) [4]. A slightly lower value of κl in PbTe films compared with the bulk crystals [4] may be due to phonon scattering on structure defects (vacancies, interstitial atoms). The role of phonon scattering on the block boundaries and surfaces is negligible, which follows from the fact of the practical absence of dependence κl on the thickness of the film (0.5–5 μ). This indicates a small value of the average free path of phonons at temperature $T = 300$ K.

4. Conclusions

The technological parameters for the fabrication of *n*-PbTe films by the evaporation method were optimized aiming to obtain a high thermoelectric figure of merit. In order to measure the Seebeck coefficient in thin films at temperature $T \sim 300$ K a set up was developed providing the accuracy of the Seebeck measurement on the level of 1%.

A wide range of film samples with electron concentration from $n = 8 \times 10^{16}$ cm^{-3} up to 2×10^{18} cm^{-3} was obtained by variation from the stoichiometric PbTe composition and using PbTe doped with iodine impurity.

A systematic study of transport properties (Hall coefficient R_H, Seebeck coefficient *S*, electric conductivity σ, transverse Nernst coefficient *Q*) over the entire temperature range (80–400 K) for *n*-PbTe films has been performed. The density of states effective mass and mechanism of carrier scattering for *n*-PbTe films have been estimated at temperature $T = 100$ K. The value of the effective mass m^*/m_o is varied from 0.24 to 0.26, which is close to a value of *n*-PbTe bulk crystals. At this temperature, the scattering on acoustic phonons is the dominant mechanism for *n*-PbTe films.

The thermoelectric properties (Seebeck coefficient *S*, electrical conductivity σ, thermal conductivity κ) were measured at $T = 300$ K on *n*-PbTe films on a mica substrate. The calculated thermoelectric figure of merit *Z* for the best films achieved the value $Z \approx 1.3 \times 10^{-3}$ K^{-1} at 300 K, which was close to *Z* for *n*-PbTe bulk crystals. Such a high thermoelectric figure of merit *Z* for *n*-PbTe films at 300 K opens new horizons for fabrication of the Film Thermoelectric Modules (FTEM).

Declaration of competing interest

The authors declare that they have no known competing financial interests or personal relationships that could have appeared to influence the work reported in this paper.

CRediT authorship contribution statement

B. Dzundza: Conceptualization, Software. **L. Nykyruy:** Formal analysis, Data curation. **T. Parashchuk:** Writing - original draft, Writing - review & editing. **E. Ivakin:** Investigation, Software. **Y. Yavorsky:** Visualization, Software. **L. Chernyak:** Resources, Supervision. **Z. Dashevsky:** Methodology, Supervision.

Acknowledgments

This research was supported by the Ministry of Education and Science of Ukraine for young scientists "Technology of thin-film thermoelectric micro modules based on multicomponent compounds with quantum-size effects" (the state registration number 0119U100062).

Appendix A

The Seebeck coefficient is measured on a constructed automated installation with a block diagram shown in Fig. 7. During the measurement, each end of the film sample 1 is installed between two massive copper radiators 2 and 3. Two differential thermocouples 5 are inserted into the radiators through ceramic tubes to exclude electrical contact. Thin layers of indium 6 were used as ohmic contacts. Hot water is passed through two radiators on one side, and cold water is passed through the other side. The set temperatures of both hot and cold water are maintained by the microcontroller using the developed thermostats. The water is heated using an electric heater. The cooling thermostat is designed on the basis of 12 V Peltier elements. The power in the heating and cooling mode is set up independently by PWM modulation using a proportional-integral-differential temperature stabilization algorithm. To minimize interference, both the heater and the Peltier elements are switched on via LC filters. The feedback is carried out using digital temperature sensors with I2C interface. The heat removed from the hot side of the Peltier elements is carried out by an air fan. Both thermostats maintain the set temperature with an accuracy of 0.1 °C.

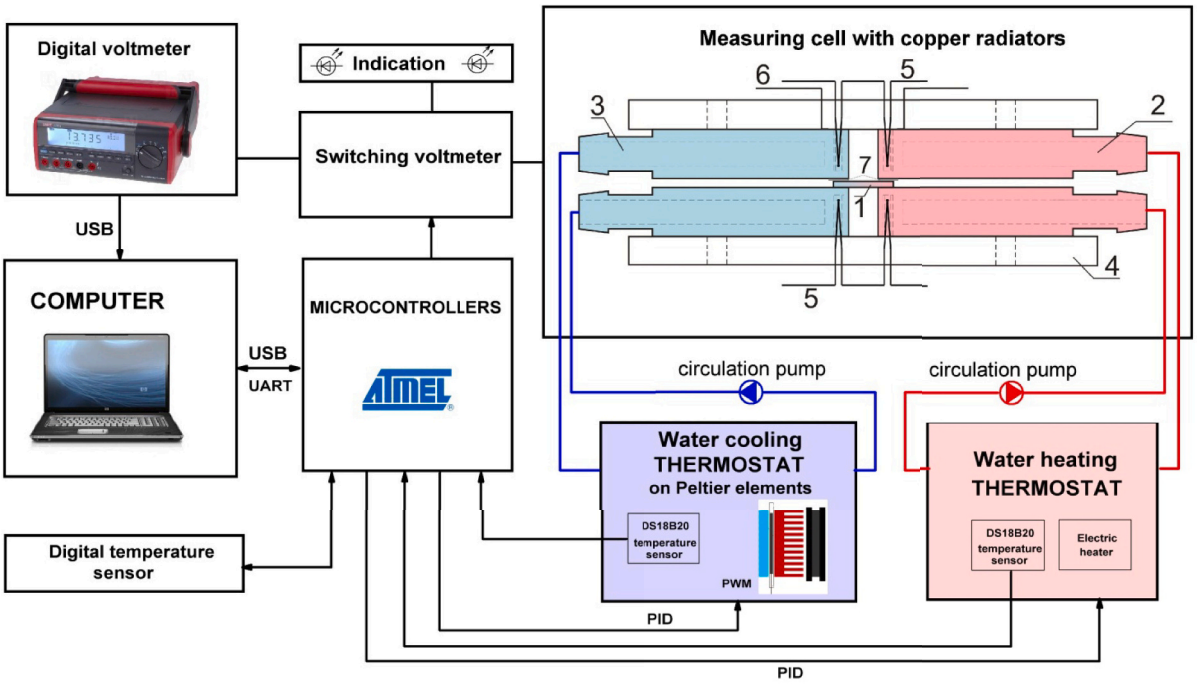

Fig. 7. Schematic view of set up for Seebeck coefficient at thin films and a scheme of measurement apparatus. 1 -sample, 2 - copper radiators, through which hot water is passing, 3 - copper radiators, through which cold water is passing, 4 - isolated plate, 5 - differential thermocouples Cr–Al, 6 - thin indium contact layer, 7 - electrical contacts.

Appendix B

The transport properties measurements on thin films over the entire temperature range (10–500 K) performed using the developed setup adapted for the liquid-helium temperatures. For the measurement, a film should be placed in a holder with six measuring probes 12–17 (Fig. 8 (a)). Sample 3 should be clipped between two massive copper plates 1–2. The average temperature is measured using a thermocouple 8 connected to the copper plate 1. The temperature gradient has been measured by high-precision differential Cu–Cu(Fe) thermocouples with wire diameter 0.1 mm. Fig. 8(b) shows the cryostat for low temperatures, which is made from stainless steel with reservoirs for liquid nitrogen 19 and liquid helium 26. The intermediate temperatures between the helium and the room temperatures were achieved by heater 23, which is wound on the cylinder of the copper plate 1.

The measurement of voltage drop on the sample, reference resistor, Hall, and current contacts is carried out sequentially with the help of six reed micro relays of the switching unit. A stable current generator is implemented on an LM234 chip by the template and has 12 discrete current values controlled by an ammeter.

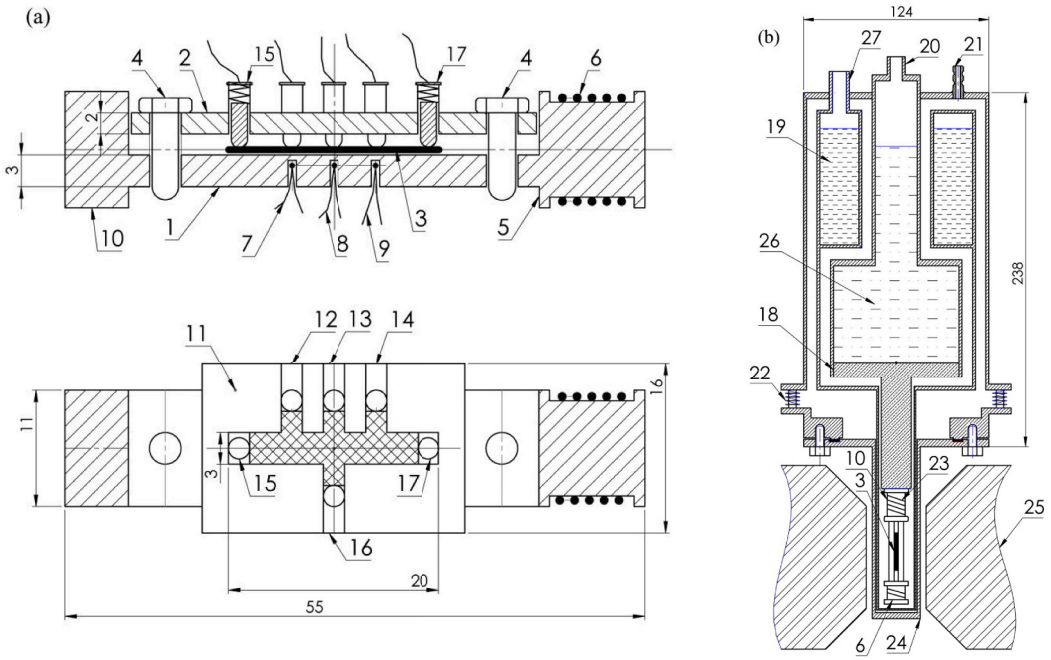

Fig. 8. Schematic view of the device for transport properties measurements on thin films over the entire temperature range (10–300 K). (a) - measurement cell, (b) - cryostat. 1, 2 – copper plates, 3 – sample, 4 – clamping bolts, 5, 10 – heat transfer tubes, 6 – gradient heater, 7–9 – thermocouples, 11 – mica plate, 12–17 - measuring probes, 18 – copper bottom, 19 – reservoir for liquid nitrogen, 20 – nozzle for liquid nitrogen filling, 21 – nozzle for pumping out, 22 – vacuum connector, 23 – heater, 24 – removable cover, 25 – electromagnet core, 26 – reservoir for liquid helium, 27 – nozzle for liquid helium filling.

Appendix C

The layout of the experimental setup for the investigation into the thermal properties of the films is shown in Fig. 9. Investigation into heat transfer is carried out by the method of transient gratings, which suggests that the sample absorbing the light is excited by two mutually interfering beams of laser radiation [23]. The spatial-periodic effect on the sample forms a transient diffraction grating in it, which is probed by a continuous laser. The damping kinetics of the diffraction signal is subjected to investigation.

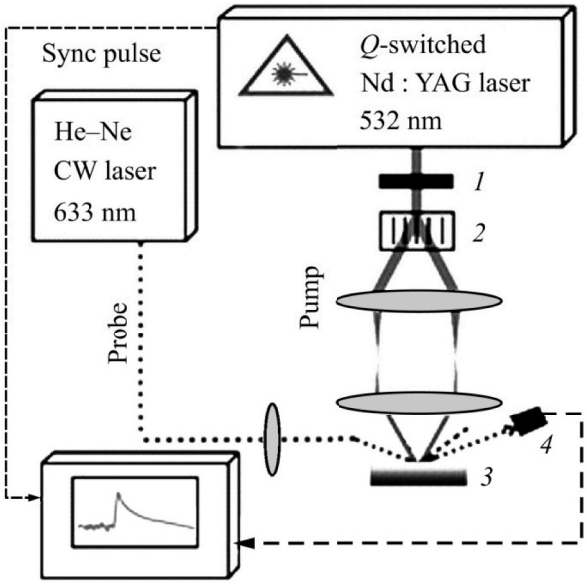

Fig. 9. Setup for measurements of thermal conductivity. 1 - attenuator, 2 - diffraction light splitter, 3 - sample, 4 - photodetector.

References

[1] A.D. Lalonge, Y. Pei, H. Wang, J. Snyder, Lead telluride alloy thermoelectrics, Mater. Today 14 (2011) 526–532.

[2] Z. Dashevsky, in: D. Khokhlov, Talor&Francis (Eds.), The Applications of Lead Chalcogenides in Thermoelectric Devices, Lead Chalcogenides: Physics and Application, 2003. New York.

[3] T. Parashchuk, Z. Dashevsky, K. Wojciechowski, Feasibility of a high stable PbTe:In semiconductor for thermoelectric energy applications, J. Appl. Phys. 125 (2019) 245103.
[4] Yu I. Ravich, B.A. Efimova, I.A. Smirnov, Semiconducting Lead Chalcogenides, Plenum Press, New York, 1970.
[5] J.P. Heremans, C.M. Thrush, D.T. Morelli, Phys. Rev. B, Thermopower enhancement in lead telluride nanostructures 70 (2004) 115334.
[6] Y. Gelbstein, Z. Dashevsky, M.P. Dariel, Physica B, High performance *n*-type PbTe-basedmaterials for thermoelectric applications 363 (2005) 196–205.
[7] D. Ben-Ayoun, Yatir Sadia, Y. Gelbstein, Compatibility between Co-metallized PbTe thermoelectric legs and an Ag–Cu–in brazing alloy, Materials 11 (2018) 99.
[8] X.-K. Wang, I. Veremchuk, M. Bobnar, J.-T. Zhao, Yu Grin, Solid solution $Pb_{1-x}Eu_xTe$: constitution and thermoelectric behavior, Inorg. Chem. Front. 3 (2016) 1152–1159.
[9] Yi Xia, J.M. Hodges, M.G. Kanatzidis, M.K.Y. Chan, Revisiting lattice thermal transport in PbTe: the crucial role of quartic anharmonicity, Appl. Phys. Lett. 112 (2018) 181906.
[10] J.R. Sootsman, D.Y. Chung, M.G. Kanatzidis, Angew. Chem. Int. Ed. 48 (2009) 8616.
[11] Z. Dashevsky, S. Skipidarov, Investigating the performance of bismuth – antimony telluride, in: S. Skipidarov, M. Nikitin (Eds.), Novel Materials and Device Design Concepts. Thermoelectric Power Generation, Springer, New York, 2019.
[12] B.M. Goltzman, Z.M. Dashevsky, V.I. Kaydanov, N.V. Kolomoetz, Film Thermoelements: Physics and Application, Nauka, Moscow, 1985 (in Russian).
[13] P. Fan, Z. Zheng, Z. Cai, T. Chen, P. Liu, Appl. Phys. Let., in: The High Performance of a Thin Film Thermoelectric Generator with Heat Flow Running Parallel to Film Surface, vol. 102, 2013, 033904.
[14] Q. Wu, J. Hu, Smart Materials, and Structures, A Novel Design for a Wearable Thermoelectric Generator Based on 3D Fabric Structure, vol. 26, 2017, 045037.
[15] R.J.M. Vullers, R. Schaijk, I. Doms, C. Hoof, R. Mertens, Micropower energy harvesting, Solid State Electron. 53 (2009) 684–693.
[16] M. Mizushiri, M. Mikami, K. Ozaki, K. Kobayashii, Thin-film thermoelectric modules for power generation using focused solar light, J. Electron. Mater. 41 (2012) 1713–1719.
[17] K. Tappura, Kaarle Jaakkola, Proceedings, A thin-film thermoelectric generator for large-area applications 2 (13) (2018) 779.
[18] M. Penhaker Proto, S. Conforto, M. Schmid, Nanogenerators for human body energy harvesting, Trends Biotechnol. 35 (2017) 610–624.
[19] K. Settaluri, H. Lo, R.J. Ram, J. Electron Mat, Thin thermoelectric generator system for body energy harvesting 41 (2017) 984–988.
[20] L. Palmetshofer, Ion implantation in IV–VI semiconductors, Appl. Phys. A 34 (1984) 139.
[21] M.P. Dariel, Z. Dashevsky, A. Jarashnely, S. Shusterman, A. Horowitz, Carrier concentration gradient generated in p-type PbTe crystals by unidirectional solidification, J. Cryst. Growth 234 (2002) 164–170.
[22] I.V. Horichok, T.O. Parashchuk, Point defects in PbCdTe solid solutions, J. Appl. Phys. 127 (2020), 055704.
[23] E.V. Ivakin, I.G. Kisialiou, L.I. Nykyruy, Y.S. Yavorsky, Optical studies of heat transfer in thin films PbTe:Bi(Sb), J. Semiconduct. 52 (2018) 169–174.
[24] Z. Dashevsky, A. Belenchuk, O. Shapoval, E. Gartstein, PbTe films grown by hot wall epitaxy on sapphire substrates, Thin Solid Films 461 (2004) 256–265.
[25] G. Springholz, Molecular Beam Epitaxy of IV-VI Semiconductors. Low Dimensional Structures and Device Applications, Elsevier Inc., Amsterdam, 2018.
[26] D.L. Young, T.J. Coutts, V.I. Kaydanov, Density-of-states effective mass and scattering parameter measurements by transport phenomena in thin films, Rev. Sci. Instrum. 71 (2000) 462–466.